IMPROVEMENTS IN LOW FIELD MRI

An Undergraduate Research Scholars Thesis

by

STEPHEN E. OGIER

Submitted to Honors and Undergraduate Research
Texas A&M University
in partial fulfillment of the requirements for the designation as

UNDERGRADUATE RESEARCH SCHOLAR

Approved by
Research Advisor: Dr. Steven M. Wright

May 2013

Major: Electrical Engineering

TABLE OF CONTENTS

Page

ABSTRACT

Improvements in Low Field MRI. (May 2013)

Stephen E. Ogier
Department of Electrical and Computer Engineering
Texas A&M University

Research Advisor: Dr. Steven M. Wright
Department of Electrical and Computer Engineering

The world of clinical magnetic resonance imaging (MRI) is presently dominated by multi-million dollar machines that use large superconducting magnets to generate very high quality images. It is possible to perform MRI at lower magnetic field strengths, which allows the use of lower-cost permanent or resistive magnets. Unfortunately, working at lower field strengths comes at a cost, as the intensity of the magnetic resonance signal is much lower at low magnetic fields. Although low fields were common in the early days of MRI, they have since become displaced by scanners with much higher field strengths. Today, advances in MRI such as prepolarized and hyperpolarized imaging are making low field strengths attractive once again,

This research presents work devoted to three problems in low-field MRI. The first development is in the use of non-phase stable receivers. Phase stability in an MR receiver is necessary if phase-encoded imaging, the industry standard, is to be used. Our lab had previously developed a desktop MRI system, but the receiver was not phase stable. By digitizing the second RF pulse in the pulse sequence, it is possible to extract information about system delays to correct for phase shifts, rendering the system phase stable.

A second effort is the development of a simple single-axis gradient set to better allow slice selection. The stronger gradient allows for the selection of thin slices with RF pulses of reasonable length.

The third effort was in low-noise RF coils. By developing an RF coil that rejects external noise, it would be possible to greatly reduce the size and cost of low-field MRI systems by the need for RF screening. We were able to acquire images successfully without the use of an RF shield using an RF gradiometer coil.

In addition, an investigation was made into moving the desktop MRI system into the fringe field of a large superconducting magnet. Although this experiment was unsuccessful in producing a detectable spin echo, a great deal of knowledge about the limitations and difficulties of fringe-field MRI was gained in the process.

DEDICATION

Soli Deo gloria

ACKNOWLEDGMENTS

I would like to thank Dr. Wright for his support and guidance throughout this project. I would also thank Dr. John Bosshard and Neal Hollingsworth for answering an incredible number of questions during every step of this project.

NOMENCLATURE

$\mathbf{B}_0$	Static Magnetic Field
$\mathbf{B}_1$	Radiofrequency Magnetic Field
CT	Computed Tomography
EPI	Echo Planar Imaging
IF	Intermediate Frequency
LNA	Low Noise Amplifier
MRI	Magnetic Resonance Imaging
NMR	Nuclear Magnetic Resonance
PET	Positron Emission Tomagraphy
RF	Radiofrequency
SEA	Single Echo Acquisition
SENSE	SENSitivity Encoding
SMASH	SiMultaneous Acquisition of Spatial Harmonics
SNR	Signal to Noise Ratio
SQUID	Superconducting Quantum Interferance Device

CHAPTER I

INTRODUCTION AND AIMS

This thesis presents the study of imaging techniques for MRI in low magnetic fields. The aim of this research is to develop a low cost system that is capable of producing quality images in an open magnet with low fields. This is accomplished through several means. First, a previously developed system was extended to create phase stability, which is crucial for phase-encoded imaging. Second, an additional gradient coil was built to improve the gradient strength capability of the system in the slice select direction and demonstrate the capabilities of a new design. Lastly, an RF Gradiometer coil was developed to allow for the supression of radiofrequency noise without the use of a screened room or chamber. In addition, an experiment was perfomred testing the behavior of the spectrometer in the fringe field of a permanent magnet.

Motivation

The field of clinical MRI is currently dominated by multi-million dollar machines that require large, superconducting solenoidal magnets to generate the strong, homogeneous magnetic fields that are required for traditional imaging techniques. Almost all clinical MRI is performed using Fourier based imaging and reconstruction, even in accelerated techniques such as EPI [1]. These imaging techniques require very homogeneous fields and expensive, low-noise, phase-stable receivers. In addition, MR suites are typically shielded from external RF fields with an expensive conductive chamber in the imaging suite.

By using phase stability correction and the RF gradiometer coil, it is possible to perform imaging without the use of a phase-stable receiver or an RF shielded chamber. This would greatly simplify the hardware needed to perform MRI with low-field magnets. By using

alternative data collection and reconstruction techniques, it is possible to greatly eliminate the dependence on superconducting magnets. Through the methods demonstrated in this thesis, it may be possible to perform imaging in low fields which need not be totally homogeneous. In fact, it is possible to perform imaging with single-sided magnets, which produce a magnetic field with a permanent gradient.

Magnetic Resonance Imaging

Magnetic Resonance Imaging (MRI) is a non-ionizing, non-invasive tomographic imaging method that uses magnetic fields and radio-frequency (RF) pulses to generate images. MRI uses the Nuclear Magnetic Resonance (NMR) phenomena to generate a signal that has information about the sample encoded in it. MRI is most commonly used in a clinical setting, where over the last few decades it has become invaluable in the diagnosis of a wide variety of ailments.

The NMR phenomenon has been used to elicit chemical spectra for over fifty years. Dr. Lauterbur [2] first introduced MRI in the 1970's. At first, frequency encoding was used to acquire projections from various angles, which were reconstructed in a manner very similar to that used in CT. It was soon realized that the NMR experiment (the gradient and RF pulses) could be constructed in a way such that the data collected was the 2-D Fourier Transform of the portion of the specimen being imaged. This technique is known as phase encoding, and is used today in the vast majority of MRI images.

The basic MRI scanner consists of four major parts. First, a large magnet is needed to produce the static that alligns the spins in the sample. Next, an RF transmitter is needed to generate pulses to excite the spins in the sample. Additionally, a set of spatially varying electromagnets are needed to create a gradient in the magnetic field. Lastly, a receiver is needed to digitize and process the signal generated by the NMR experiment.

MRI has several advantages over other imaging modalities, such as computerized tomography (CT), and positron emission tomography (PET). First, MRI uses non-ionizing radio-frequency waves, which are incapable of damaging cells, to perform imaging. On the other hand, CT scans require large X-ray doses, and PET requires the injection of radioactive contrast agents that produce gamma rays, which when detected are used to form images. In addition, MRI has excellent soft tissue contrast in comparison to CT, which is less capable of imaging soft tissue, and PET, which provides almost no structural information. Lastly, the MRI contrast mechanism is flexible, and with various techniques, MRI can easily be used to distinguish or suppress fluids [3], fat and water [4], and diffusion [5].

Parallel MRI

In the early 90's parallel imaging was introduced as a means to reducing scan time [6]. By using multiple receiver coils, it is possible to reduce the number of phase encode steps needed to acquire an image, reducing scan time for a given image resolution. Over the next several years, several methods were developed to do this. The theory of parallel MRI is based on the use of multiple receiver channels with multiple coils. Each coil in the receive array exhibits a different sensitivity pattern and provides unique information about the sample. When performing parallel imaging, lines of k-space are skipped, reducing scan time. These lines are recreated using data from the parallel receivers and knowledge of the spatial sensitivities of the coils in the array. Parallel imaging is capable of reducing imaging time by a factor equal to the number of independent receive channels, with only a slight reduction in SNR.

One of the first techniques developed to do this is called SMASH [7]. This technique uses a linear array of spatially separated coils to allow the missing phase encoding steps to be recreated using weighted sums of the information from the array of coils. Later, a more flexible technique entitled SENSE was developed [8]. This technique is more flexible and allows for arbitrary coil configurations and k-space sampling patterns.

One of the chief difficulties with parallel imaging is decoupling the coils used in the receive array. It is important to minimize the mutual impedance of the coils in the array in order to ensure that the coils are truly independent. This is necessary because in order for the coils to acquire unique information about the subject, they need to be completely decoupled - any mutual impedance between the coils will cause them to record some of the same information. In order for parallel reconstruction techniques to work, independent data is neede from each coil.

Here at Texas A&M, the Magnetic Resonance Systems Lab (MRSL) has worked to extend parallel imaging to it's furthest extreme. A technique has been developed to use an array of 64 very narrow coils to eliminate phase encoding entirely. The wide array of coils cover the entire field of view, allowing for an entire image to be acquired in a single echo. This technique is fittingly called Single Echo Acquisition [9]. In addition, because an entire image can be acquired in the time it takes to generate and record a single echo, it is possible to achieve very fast imaging rates using gradient echo and recalled echo sequences.

Low Field MRI

Often, the largest part of an MRI system is the magnet used to produce the static $\mathbf{B}_0$ field. In a modern clinical scanner, the magnet can account for half of the cost of the system. In the early days of MRI, low field magnets were common, even clinically (the .06T magnet used to perform these experiments used to belong to a hospital). Now, almost all clinical scanners are built with either 1.5 or 3 T superconducting magnets. The MR signal is proportional to the square of $B0$, which gives a clear advantage to superconducting magnet systems, which have an enormous increase in SNR over permanent magnet systems.

Low field MRI retains several major advantages over conventional clinical MRI. First, the frequency of operation is much lower for low field systems. The .06T system operates at approximately 2.46 MHz, while a 3T system operates at closer to 128 MHz. This greatly

relaxes requirements for the system hardware and makes possible receiver techniques such as direct digitization (without any IF stages) and undersampling. Second, the lower frequency results in a much longer wavelength, which makes it possible to construct RF coils (such as the multi-turn gradiometer) that would be impossible at higher frequencies. Lastly, magnets are much easier to construct at low fields, and $\mathbf{B}_0$ inhomogeneity is much less of a concern at lower fields.

There are some exciting possibilities developing in MRI that make help eliminate the SNR problems found in low-field MRI. The first of these is hyperpolarized MRI, where Dynamic Nuclear Polarization is used to greatly increase the polarization of the spins in an MRI sample. Typical polarizations for proton (Hydrogen) imaging are 9.9 ppm at 3T and .40 ppm at .06T. Hyperpolarizing the spins can result in polarizations of up to 50%, which more than compensates for the losses due to low field strength. In fact, Hyperpolarized MRI is better performed at low fields, as the spins relax back to their equilibrium state (by T_1 relaxation) more slowly at low fields.

The other technique that shows promise in improving performance at low fields is Prepolarized MRI. In this technique, a strong, pulsed magnetic field is used to polarize the spins in the sample while RF excitation is applied. This pulsed field is turned off, and a weaker, more homogeneous magnetic field is used during readout [10]. The strong prepolarization pulse (often .5T) increases the polarization of the sample, and reading out at a lower field allows a less expensive, more homogeneous magnet to be used to acquire the image data.

Single Sided MRI

One of the other major limitations of MRI is the requirement of a strong, homogeneous magnetic field. These magnets typically make up at least half the cost of a clinical MRI system, and keeping the magnet superconducting (whether by frequent filling of cryogens or powerful helium recompressors) is a major expense. Some of the first work on different

magnet structures was done in the field of oilfield logging [11]. Since then, much work has been done in using single sided magnets, which can be used to image objects much larger than the magnet. Blümich, Casanova, and others [12, 13] have developed a system using a single sided magnet. This system was initially designed to perform spectrum and relaxation time measurements, but it has been extended to be capable of performing two-dimensional imaging.

The most important feature (and limitation) of a single sided magnet is a permanent gradient field in the direction normal to the surface of the magnet. This change in field strength can cause problems, as it prevents the use of gradient echo sequences and precludes frequency encoding in a direction other to that normal to the surface of the magnet. This gradient can, and is, used to perform slice selection with the rf pulses, but the fixed gradient strength limits the flexibility of slice thickness.

A great deal of work has been done in the stray fields of superconducting clinical magnets [14]. The fringe-fields of a superconducting magnet are extremely uniform in places. The fields decay as one moves further from the magnet, which allows the strength of the fields used to be varied as needed. Using the fringe fields of a superconducting magnet is very good for research, but it doesn't remove the need of a large superconducting magnet. In addition, there is limited flexibility in the direction of magnetic field. The region of highest homogeneity typically has a magnetic field in a direction orthogonal to that of the permanent gradient. This may prevent the use of some types of RF coils, as the $\mathbf{B}_1$ (RF excitation) field needs to be orthogonal to the $\mathbf{B}_0$ (static) field.

Systems like the NMR-MOUSE use a custom built permanent magnet [12, 13]. This allows the magnetic field to be tailored to the need of the system. Although they also have a static field that is orthogonal to the gradient, it is conceivable to devise a system in which the static field is in the same direction as the gradient.

Research Objectives

The aim of this work is to extend existing work in low-cost, low-field MRI systems to allow different types of imaging and lay groundwork for future developments in highly parallel imaging in similar systems. There are three specific aims towards this goal. They are concerned with the enhancement and expansion of desktop MRI system that was previously developed in our lab.

Phase Correction on the Desktop MRI System

The first step in expanding the capabilities of the desktop MRI system previously developed is making adjustments to the system to ensure phase stability. In order for any of the standart imaging techniques to be used with this system, it is necessary to modify the system to collect enough data such that phase instabilities can be corrected. In addition, after these changes are made, new pulse sequences will be written that allow phase-sensitive imaging techniques to be used on the system.

.06 T System Development

The next step is to apply the desktop system for use with a larger permanent magnet. This will require the construction of a new RF coil and gradient set and adapting existing equipment to work on a larger scale. The gradient set will require simulation during the design process in order to ensure the quality of the fields it will produce. The RF gradiometer coil will reject external noise, allowing the system to perfrom imaging without electromagnetic screening.

Fringe Field Imaging

The last step is the demonsration of the desktop spectrometer when the coil and phantom are placed in the fringe field of a large superconducting magnet. Although it is possible to find a spot in the fringe field of the magnet that has the same static field strenght as that of the permanent magnet, difficulties are presented by the strong permanent gradient field in the fringe field of the magnet. Although this particular experiment was unsuccessful in acquiring an echo, it did result in a wealth of knowledge about the limitations of fringe field imaging.

CHAPTER II

BACKGROUND

In this chapter, the basic theory behind MRI will be presented. This will in no way be an exhaustive introduction[1], but it is simply meant to provide an overview of the principles on which MRI is based. In addition, background information on the desktop MRI system used as a basis for this research will be given.

Magnetic Resonance Imaging

Magnetic Resonance Imaging (MRI) is an imaging technique that uses pulses of radiofrequency and gradient magnetic fields to elicit information about the structure of an object. MRI has seen widespread use in medical imaging, where it is valued for its ability to generate detailed images of soft tissue. In this section, an introduction to the physics and principles of MRI will be presented beginning with the physics of Nuclear Magnetic Resonance. The imaging process will then be introduced, and the components of an MRI system will be also introduced.

Nuclear Magnetic Resonance

Magnetic Resonance Imaging is based on the Nuclear Magnetic Resonance phenomenon, which involves the behavior of protons when placed in a magnetic field. When placed in a static magnetic field, known in MRI as $\mathbf{B}_0$, the spins of the protons align (at an angle) either parallel or anti-parallel to the static magnetic field and begin to precess about the direction of the magnetic field at a characteristic frequency. This frequency, known as the Larmour

[1]The following information can be found in greater detail in any medical imaging text, such as [15]

Frequency, is proportional to the applied magnetic field. The relationship between $\mathbf{B}_0$ and the Larmour Frequency is expressed as:

$$\omega = \gamma \mathbf{B}_0 \tag{II.1}$$

where ω is angular frequency (radians per second) of precession and γ is the gyromagnetic ratio, which varies depending upon the nucleus under interrogation. For Hydrogen H_1^1, the gyromagnetic ratio is 42.5759MHz/T.

The two spin states that the protons align to (parallel and anti-parallel) have slightly different energies, so slightly more spins occupy the lower-energy parallel state. When a large number of spins are considered, this population difference generates a net magnetization $\mathbf{M}$ that is aligned with the $\mathbf{B}_0$ field.

If the spins are exposed to a time-varying magnetic field $\mathbf{B}_1$ at the Larmour Frequency, then the net magnetization will be tipped into the transverse plane. The angle that the spins are tipped to is proportional to the $\mathbf{B}_1$ field, which is often calibrated to give a 90°tip. The precessing net magnetization will then produce a signal at the Larmour Frequency, as all of the magnetic moments are oscillating in phase with each other. This signal (the finite induction decay, or FID) will decay as interactions with the surrounding environment cause the tipped spins to gradually lose phase coherence, a process known as T_2 relaxation. This loss in coherence is due to two causes: random interactions with nearby atoms (T_2^*)and small permanent variations in the local magnetic field (T_2). In addition, the tipped down spins will also relax back to their un-tipped rest state, a process known as T_1 relaxation. T_1 is usually much longer than T_2, so it has little effect on the FID.

In order to extract spatial information from the sample, it is necessary to dephase the spins and bring them back into phase. The simplest way to bring the spins back into phase is to use a second RF pulse that generates twice the $\mathbf{B}_1$ field of the first pulse. This causes the tipped spins to flip 180°, reversing the non-random dephasing processes. After a time equal

to the time between the 90°and 180°RF pulses, the spins will be back in phase, generating a signal called a spin echo. Spin echoes are only capable of recovering from static local inhomogeneities, so the peak of the spin echo is still subject to T_2 decay.

Imaging

In order to perform imaging, it is necessary to encode spatial information into the echo generated by the RF pulses. This is done using additional, spatially varying magnetic fields known as gradients. These electromagnets produce a field in the same direction as $\mathbf{B}_0$, but with a variation in the X, Y, or Z direction. These fields cause the Larmour frequency to vary depending on the position of a nucleus in a manner linearly proportional to their position relative to the isocenter of the magnet.

Spatial Localization

The first way in which this is used to spatially localize the collected information is to perform slice selection. By using an RF pulse envelope with a finite bandwidth (typically a truncated sinc function) and a single gradient that causes the Larmour frequency to vary in one direction, it is possible to only excite the spins in only a slice of the sample. This makes it possible to perform tomographic imaging, as information is only collected from one slice.

Next, it is possible to spatially localize in another direction by applying a constant gradient during the echo, known as frequency-encoding. This causes a shift in the frequency of the spins proportional to the distance along the axis of the frequency-encoding gradient, generating a projection of the sample. By taking projections at multiple angles, it is possible to use backprojection reconstruction to generate an image, as Lauterbur did in 1973. However, most modern MRI systems use a different technique called phase encoding.

k-Space

Phase encoding uses gradient pulses in two directions orthogonal to each other (and to the slice select direction) to encode the 2-D Fourier Transform of the selected slice into a series of echoes which are captured by the receiver. The two-dimensional Fourier Space is known as k-space, as the baseband signal of a spin echo is commonly written as:

$$S_0(t) = \int_{-\infty}^{\infty} \int_{-\infty}^{\infty} \rho(x, y) e^{2\pi j(k_x + k_y)} dx dy \tag{II.2}$$

Where $k_x = \int \gamma G_x dt$ and $k_y = \int \gamma G_x dt$ are the phase shifts due to the gradients up to that point in time, and rho is the spatial density of spins. MRI convention has frequency encoding in the x direction and phase encoding in the y direction.

To collect a phase encoded image, multiple eches are acquired with different values of k_y. The two-dimesional array of digitized echoes is known as the k-space data, and when the 2-D Discrete Fourier Transform (DFT) of this data is taken, the image of the slice is recovered.

Pulse Sequences

The sequence of RF and gradient pulses used to perform imaging is known as a pulse sequence. For imaging to be successful, there must be precise, repeatable synchronization between the RF pulse, digitizer, and gradient waveforms. There are two principle parameters that define a pulse sequence that are adjusted to change image contrast and quality. First is Echo Time (TE), which is the time between the center of the first RF pulse and the center of the echo. The second is Repetition Time (TR), which is the time between the starts of successive repetitions of the pulse sequence. A simple spin-echo pulse sequence can be seen in figure II.1.

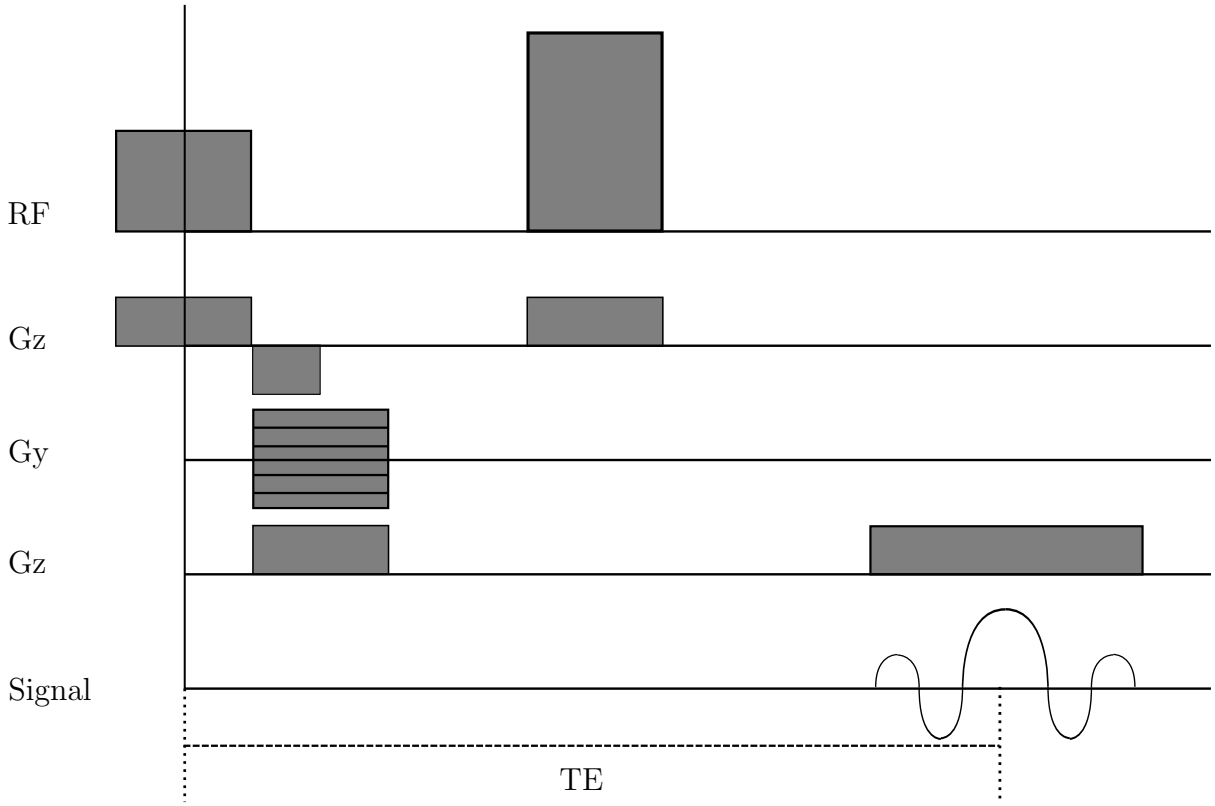

Fig. II.1. Simple spin-echo pulse sequence

System Components

The major components of an MRI system can be divided into three parts: the magnet and coils within it, the spectrometer, and the various amplifiers that interface between the two. The whole MRI system is controled by a host computer, which calculates pulse sequence parameters based on the imaging parameters selected by the user and processes and reconstructs the data collected by the receiver.

Magnet and Coils

The most easily recognizable part of an MRI system is the magnet. In clinical imaging systems, this magnet is typically a superconducting solenoidal magnet of 1.5 or 3 T. Other types of magnets do exist, and some magnets either use resistive copper windings or powerful permanent magnets. Although solenoidal magnets are almost universal in clinical imaging systems, other topologies are possible, especially with permanent magnets, which create a field in a fundamentally different way than electromagnets. Although some systems that use permanent magnets adopt different form factors [16], the .06 T permanent magnet used for these experiment adopts a cylendrical form, although the $\mathbf{B}_0$ field is in the x direction of a traditional magnet.

Within the magnet is a set of three gradient coils, which produce the afformentioned spatial variation to $\mathbf{B}_0$ that allows for spatial localization. In addition to these coils, almost all systems include several 'shim' coils used to correct for inhomogeneities in the $\mathbf{B}_0$ field.

The final part of the magnet system is the radiofrequency coil. This resonant coil creates the oscillating $\mathbf{B}_1$ field that tips the spins in the sample and detects the signal generated by the echo. There are a wide variety of coil designs, including loops and solenoids and more complicated stuctures such as bircages [17]. At low fields, the long wavelength and low inductive reactance at lower frequencies encourage the use of solenoids and multi-turn loops, which can produce very homogeneous $\mathbf{B}_1$ fields very efficiently.

Spectrometer

The spectrometer serves as the interface between the controlling computer and the other portions of the system by generating the RF and gradient waveforms and digitizing the signal received by the coil. The central part of the spectrometer is the Pulse Sequence Generator (PSG). This device takes commands from the controlling computer and uses them to control the timing of the grandient and RF waveforms. The gradient amplifiers are typically fed directly from the PSG (with either analog or digital waveforms), but the RF waveform may require mixing up to a higher frequency.

In spectrometers designed to work with high-field magnets, it is not feasible to generate the the RF waveforms at the actual Larmour frequency of the magnet (a technique known as direct digital synthesis, or DDS), so a frequency synthesiszer is used to generate the magnet center frequency, which is then modulated by waveform envelopes generated by the PSG. The use of modulation stages (many designs use two modulation stages) adds considerable complexity and cost to the spectrometer. Fortunately, at the low fields used in this work, the Larmour frequency is approximately 2.46 MHz, which is easily synthesizable by DDS. The output of the RF waveform generator is fed to the RF amplifier, which will be discussed in the next section.

The remaining parts of the spectrometer comprise the receiver. The first stage of the receiver is a low-noise amplifier (LNA) that is fed by the coil directly through the T/R switch. The signal generated by the RF coil can be very small, so it is important that the first amplification stage injects as little noise as possible. After this initial amplification stage, the signal can digitized directly, which is common at low fields, or mixed to a lower IF frequency or baseband before being digitized again.

Amplifiers and T/R Switch

The gradients and RF coils inside the magnet require a great deal of power, so it is necessary to amplifiy the waveforms from the spectrometer before they are fed into the gradient and RF coils. The gradient amplifiers operate at fairly low frequencies (40 kHz or lower) and must be capable of driving a large current (10-100 A) into an inductive load. Unlike many amplifiers (including the RF amplifier), gradient amplifiers are commonly operated in constant-current mode. Because the gradient field is proportional to the current in the coil – not the voltage across it – it is better to have the amplifier output whatever voltage is necessary to produce a current proportional to that specified by the voltage of the input waveform.

The RF amplifier serves to amplify the modulated signal from the spectrometer to whatever level is needed to tip the spins in the sample. The power required depends on the efficiency of the RF coil, which is usually inversly proportional to its size. For a sample in a small efficient coil (such as is used in .06 T system), an amplifier of 20 W is sufficient. Higher-field laboratory systems may have 1 kW amplifiers, and in clinical scanners, it is not uncommon to have an amplifier of 30-60 kW.

The last step between the transmitter and the RF coil is the Transmit/Receive (T/R) switch. This switch connects to the RF coil, the RF amplifier, and the first stage of the receiver. It serves to direct power from the RF amplifier to the coil during transmit and direct the signal from the coil to the receiver during receive. There are many ways to accomplish this task depending on the system and power levels involved. An active switch, using devices such as PIN diodes, requires power and control from the PSG to switch the coil between the two other devices. Lower power systems can use passive switches, which use ordinary diodes and phase shifting networks to automatically switch when excited by the RF amplifier. It is important that these switches are able to switch quickly, as in a fast spin-echo sequence, the time between the end of the 180°pulse and the beginning of digitization can be a few milliseconds or less.

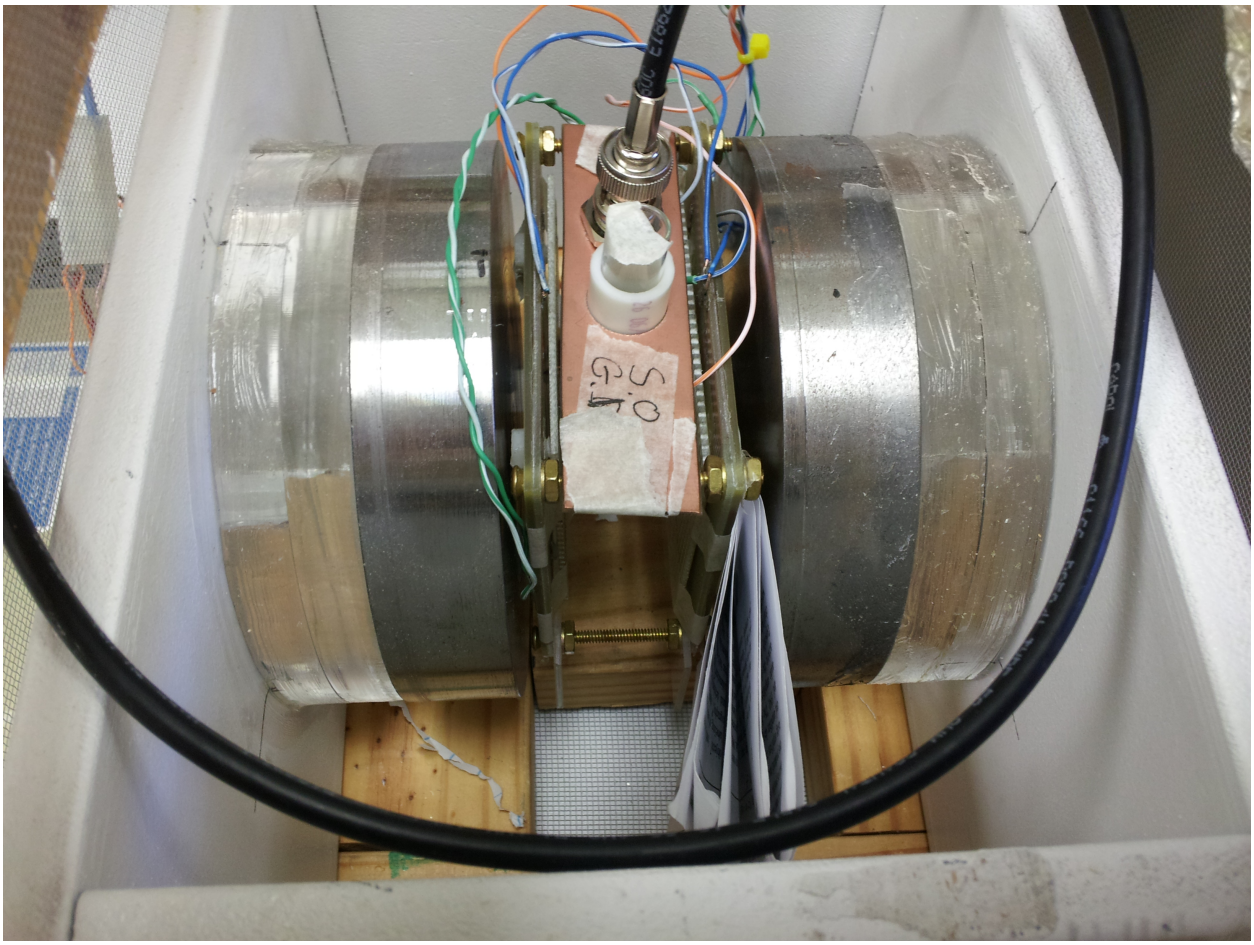

Fig. II.2. Magnet, gradients, and RF coil of desktop imaging system

The Desktop MRI System

Our lab has previously developed a simplified MRI system for use with small permanent magnets. The magnet for this system is a .08 T permanent magnet that is approximately a foot on each side. The spectrometer's waveform generation, control and digitization functions are handled by several cards manufactured by National Instruments (NI). The only additional components of the system are a blanking switch, a passive T/R switch, a 20W RF amplifier, an LNA, and a set of 3 small gradient amplifiers based on the LM-12 chip. The magnet subsystem (magnet, gradients, and RF coil) can be seen in figure II.2.

The magnet is built from two very powerful permanent magnets attached to an iron yoke. The magnetic field produced by these two magnets, which are fairly small, are spread out by two circular iron pole pieces. The magnetic field produced lies between the two pole pieces. The magnetic field produced by this magnet is approximately .08 T, but the field strength drifts some with change in temperature (a weakness that superconducting magnets do not have).

Inside the magnet, there is a set of shims/gradients for the X, Y, and Z axes. The shims were based on the design in [18], and are constructed on two sets of circuit boards–one next to each pole piece, with the RF coil in the middle. The gradient amplifiers are constant-current amplifiers based on the LM-12 high power op-amp. These amplifiers are capable of delivering 10 A and 12V and are more than capable of driving small, efficient gradient sets.

The actual spectrometer is made up of four cards built by National Instruments. The cards are a very stable clock source, a high-speed digital to analog converter (DAC) for direct digital synthesis of the RF waveform, a high-speed analog to digital converter (ADC) for digitization of the echoes from the sample after being amplified by the LNA, and a low-speed DAC for generation of the gradient and blanking switch waveforms. These cards are housed in a separate chassis that is connected to a host computer with a dedicated PCI card in that computer.

The controlling software is written in National Instruments' proprietary programing language LabView. This graphical programming language is designed to interface with NI hardware and allows users to interface with the hardware without too much low-level programming.

Projection Imaging

This system is very good, but it has one major weakness–it is not phase stable. A phase-stable system has precise enough timing such that if an echo is acquired with the same parameters multiple times, the magnitude and phase of the echoes should be identical. Unfortunatelly,

the desktop system is not phase stable–a defect which prevents it from utilizing phase encoded imaging techniques.

There is a class (ECEN 463) taught based on this system, and for this class they work around lack of phase stability of the system by performing projection reconstruction using the magnitue of the echo spectrum. By only applying a gradient in one direction, it is possible to project the 2-D phantom (sample used for test imaging) into one dimension, with the intensity at a given point on that line proportional to the sum of the signal along the line perpendicular to the read out dimesion at that point. An introductory text to medical imaging can give a more detailed explaination [15].

System Limitations

One of the first limitation of this system is its limited field of view–good images can only be acquired over a volume of about 1 cubic centimeter. Because the samples are very small, they contain a small number of spins, providing a very weak signal. The weakness of the signal makes averaging necessary, greatly increasing imaging time.

In addition, the homogeneity of the magnet is very poor, even in the small usable region of the magnet. Shimming (making corrections to the main magnetic field with small eletromagnets) is necessary to obtain an echo of any quality, and even shimmed, the homogeneity of the imaging region is poor.

In order to make the system simpler, projections are only carried out in one direction. In order to create a 2-D image, multiple projections are taken with the phantom rotated to different angles. Although phase encoding is almost standard in clinical MRI, projection imaging still has some use, but on these systems, it is the direction of projection–not the sample–that is rotated.

In order to acquire projections in different directions by rotating the readout direction, it is required to very precisely know the efficiency of the gradient coils so that the projections will

truly be acquired at the same resolution. If one gradient is stronger than the other (which is the case in the desktop system) and this is not corrected for, then the projections along that direction will be at a higher resolution making image reconstruction impossible.

The aims of this research are to overcome the limitations of the desktop system in various ways. This will be done by correcting for phase instabilities in the receiver, adapting the system to work in a large permanent magnet that allows a larger field of view, and adapting the system to operate in the fringe-field of a permanent magnet.

CHAPTER III

PHASE STABILITY, GRADIENTS, AND RF COILS

Engineered Phase Stability

As was previously mentioned, the desktop imaging system is not phase stable. Figure III.1 shows the spectra of unrephased echoes. These spectra were generated by taking a small subset of the Fourier Transform of each echo. The angles of each echo was then calculated relative to that of the first echo. The figure clearly shows substantial differences in phase between subsequent acquisitions. The relative phases fall into six clear groups, which implies that the timing inaccuracy is some multiple of a system constant. This could quite possibly be caused by the system performing a bitwise AND operation of the trigger with a clock before beginning the digitization of the echo.

Although this instability is acceptable (but still undesirable) for performing back-projection reconstruction, there is no way to perform phase encoding without phase stability. 2-D images – phase encoded in one direction and frequency encoded in another – are the gold standard of MRI, and almost all advanced or accelerated imaging techniques are based on these methods. Fortunately, because of the way the LabView software and NI hardware work, this phase instability can be corrected.

One way to correct for the phase difference between echoes is to also digitize something with known phase. In order to do this on a single channel receiver such as ours, it is necessary to acquire both the reference and the echo in the same acquisition. Fortunately, the RF pulses are the same for each acquisition, and therefore can be used as a phase reference. In order to correct for the phase instability, the digitizer is started immediately before the 180°RF pulse and run continuously until the end of the echo. The phase of the RF pulse is then used to correct the phase of the echo in post-processing.

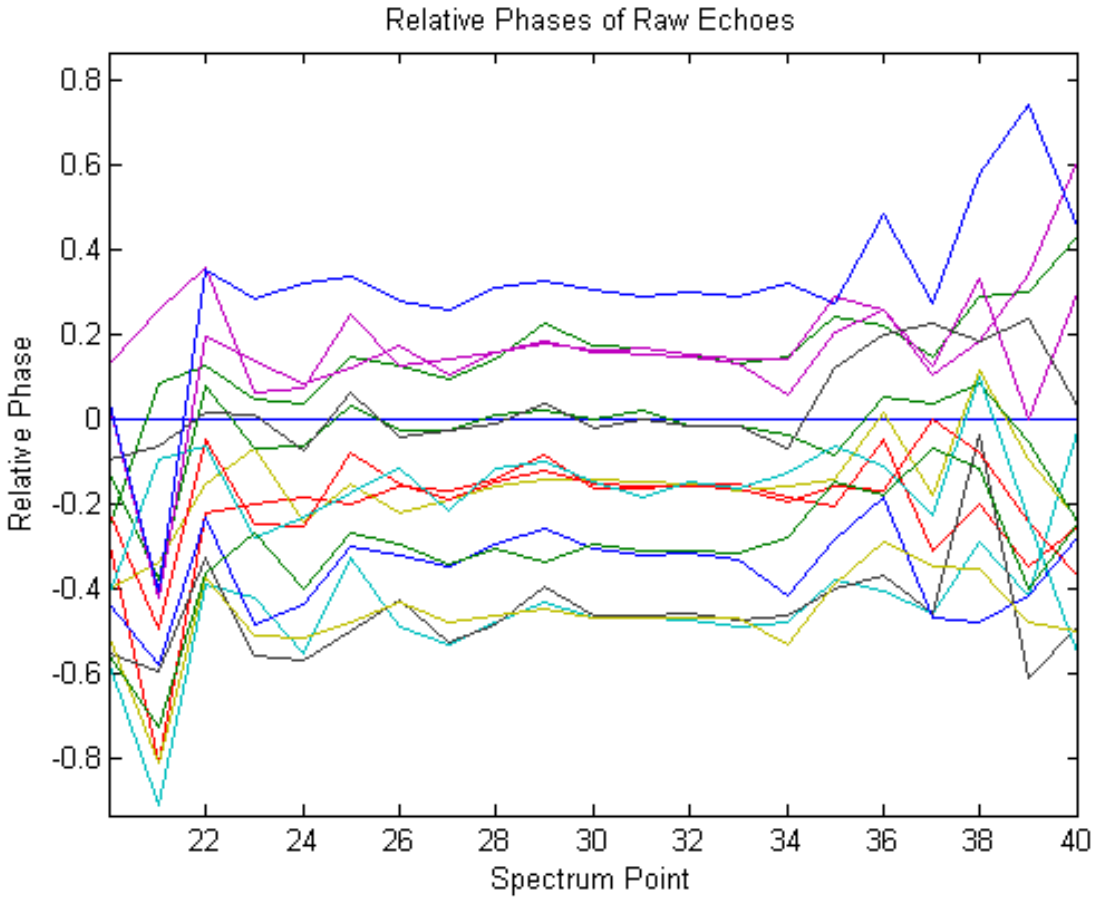

Fig. III.1. Relative phases of the spectra of uncorrected echoes.

Hardware Considerations

In order to perform phase correction using this method, the RF pulse needs to be present at the input of the digitizer during transmit. In an ideal TR switch this is impossible, as all of the power from the RF amplifier is directed to the RF coil. Fortunately, the passive TR switch used in this system is far from ideal, and a distorted version of the RF pulse is present at the input of the digitizer even during transmit. This can be attributed to the non-ideal behavior of the diodes, who don't behave as perfect shorts during RF transmit. The signal across the diodes, although distorted, contains clear information about the phase of the RF pulse.

Post-Processing

Initially the entire echo was written to file, but this generated enormous data files, so the LabView software was quickly revised to save a smaller subset of data. The first step is to separate the digitized data into the RF pulse and the echo. The Fourier Transform of each part is then taken, and a subset of this spectrum centered around the transmit frequency is what is saved to disk.

The actual phase correction processing is performed in MATLAB. A program was written to take in the two raw data files (one for the RF pulses and one for the echos) and perform phase correction on them. The phase correction procedure is straightforward:

1. Calculate the index of the peak frequency of the echo
2. Separate out the phases of the RF pulses and echoes
3. Use the phase of the first RF pulse at the previously determined peak frequency as a phase reference
4. For each subsequent RF pulse, calculate the phase difference at the peak between that RF pulse and the phase reference

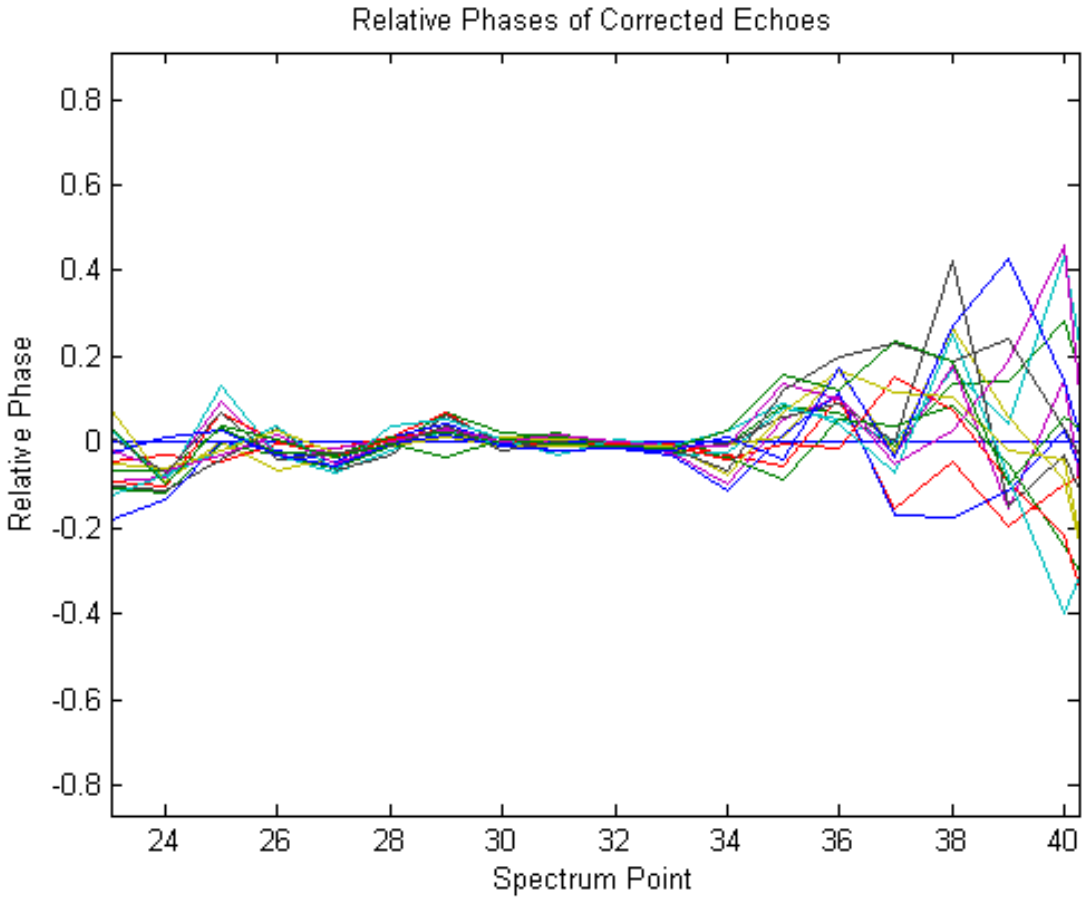

Fig. III.2. Relative phases of the spectra of corrected echoes.

5. For the corresponding echo of the each of the RF pulses shift the phase by the negative of the RF pulse phase difference

When this algorithm is applied to the echoes shown in figure III.1, the echoes in figure III.2 are obtained. Because these are echoes with no spatial encoding, it is expected that they will have nearly identical phases, which can clearly be seen in the figure.

To demonstrate the effect this has on a fully encoded image, figure III.3 was prepared, where images reconstructed without and with phase stability correction are shown. The phase stability correction does not make as large of a difference as one would expect with this

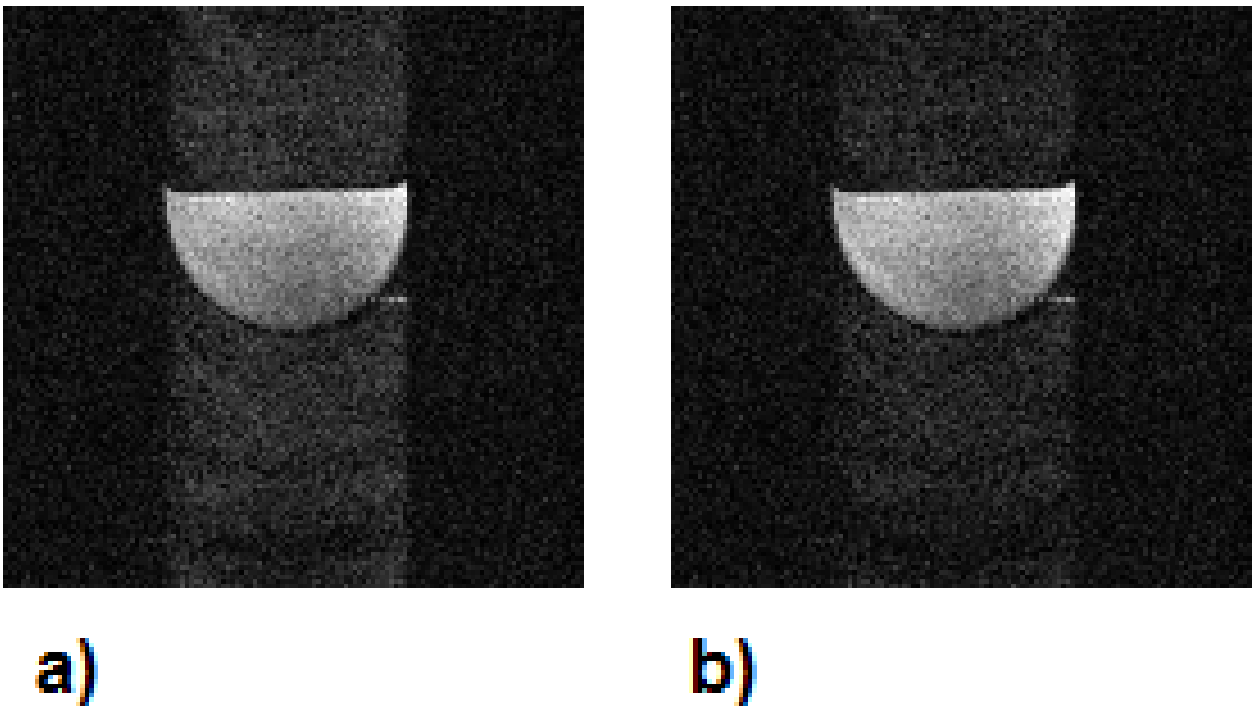

Fig. III.3. Image generated of a phantom without (a) and with (b) phase stability correction.

phantom, as most of the signal is contained in a relatively small region at the center of k-space.

An Improved Gradient System

The gradient system built into the .06 T permanent magnet used for the system was designed for whole-body imaging. These gradient coils have a large homogeneous region, but this comes at a cost – they are very weak. Table III.1 shows the gradient strengths of the built-in set. The gradient strengths were measured with a NMR probe. Projections were taken with a small vial of water with a solenoidal coil wrapped around it. By measuring the frequency

Gradient Axis	Gradient Field Strength (G/cm/A)
X	.0046
Y	.0125
Z	.0113

Table III.1
Gradient Field Efficiencies of .06 magnet system.

shift that occurred when the probe was moved along the axis of the gradient in question, it was straightforward to calculate the gradient field strengths.

Because the pulse sequence being used is a simple spin-echo sequence, there is plenty of time to use long pulses for frequency and phase encoding. Unfortunately, the X gradient[1], which is used for slice selection, is too weak to perform slice selection, which must take place during the RF pulse, which is typically 4 ms at the longest. Even running the X gradient with the maximum available current, it was only possible to obtain a 3 cm slice with a 4 ms RF pulse. Typical clinical MRI uses slices of 1cm or less, so it is necessary to change some part of the system to increase performance. The two primary options were to increase the power of the gradient amplifiers or increase the efficiency of the gradient coil. The latter option was chosen to better fit the overall aim of the project. By constructing a smaller, more efficient gradient set, it is possible to use smaller, more reasonably priced amplifiers, which also advances the goal of low-cost system development.

Traditionally, the gradient in the direction of the bore of the magnet is generated by a Maxwell Pair coil. The .06 T magnet, however, has its field directed laterally instead of down the bore, so a different gradient configuration is necessary. Commercial systems typically use fingerprint coils generated using Fourier-Bessel series [19], but for this system, a simpler Anderson coil configuration was chosen [18].

[1]The vast majority of MRI magnets which use a cylindrical magnet shape have the field directed down the bore of the magnet. Because the static magnetic field is always considered to be in the Z direction, in this system, the X direction is along the bore of the magnet.

Although Anderson provided information about the size of the homogeneous region for a gradient coil of a certain size, it was decided to simulate the gradient set to better understand the quality of the gradient fields generated. Because the gradient fields are static (i.e. they vary at an extremely low frequency from an electrical standpoint), it is possible to simulate their behavior simply using the Biot-Savart Law.

$$\mathbf{B} = \frac{\mu_0}{4\pi} \int_C \frac{Id\mathbf{l} \times \hat{r}}{|r|^2} \tag{III.1}$$

The Anderson coils are rectangular or circular loops designed to lie in two flat planes on either side of the imaging region. Because of the simplicity of this design, it is much easier to model the fields generated by the coils using a special case of the Biot-Savart Law for straight wire segments.

$$\mathbf{B} = \frac{\mu_0 \hat{\phi}}{4\pi d}(\cos\alpha_2 - \cos\alpha_1) \tag{III.2}$$

In this expression, d is the distance from the point at which the fields are being calculated to the wire segment. α_1 and α_2 are the angles at each end of the wire between the wire and the point of observation. These angles can be found using $\alpha = \cos^{-1}\frac{|l \times r|}{|l||r|}$, where l is the wire vector and r is the vector from that end point of the wire to the point of observation.

MATLAB was used to implement the simulation of the gradient coils. Figure III.4 shows the resulting plot of the field generated by the gradient coil over the field of view. When the Z component of that field is found, figure III.5 is obtained. From this plot, it can clearly be seen that the Anderson gradient set generates a gradient of .00928 G/cm/A over a spherical region of about 4 cm radius.

Once the field patterns were known, it was necessary to determine how many windings to use for each coil. This number must be a compromise, as a lower number of windings reduces the resistance and inductance of the coil, allowing it to be driven with more current and faster

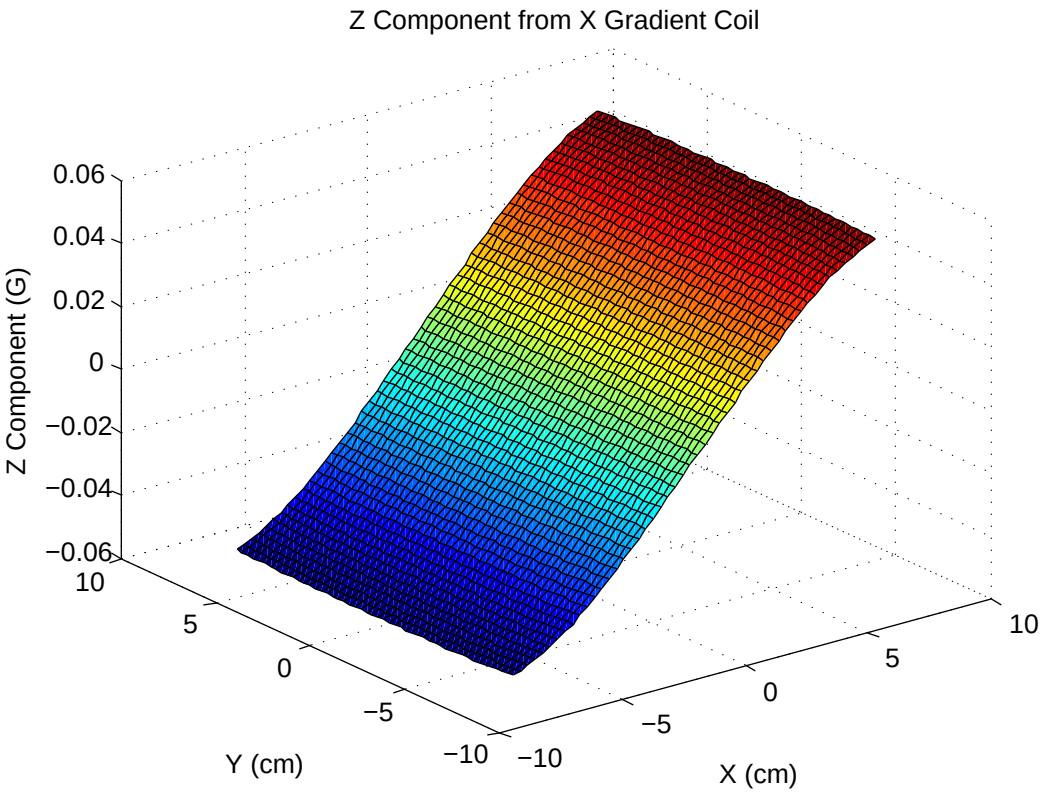

Fig. III.4. Plot of the X gradient field in the XY plane.

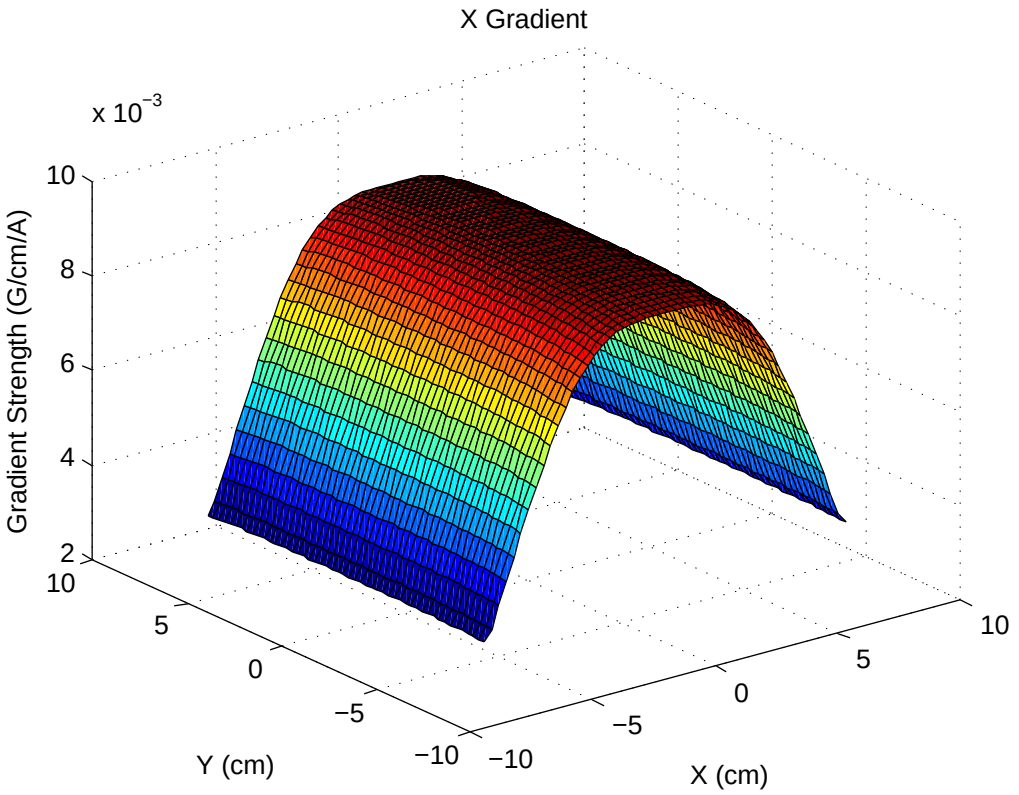

Fig. III.5. Plot of the Z component of the X gradient field in the XY plane.

rise times for a given voltage. On the other hand, a higher number of turns increases the efficiency of the gradient set, enabling a stronger gradient field to be produced with a certain current. The initial design criteria was for the gradients to be able to select a 1 mm slice thickness with a 4 ms RF pulse. A 4 ms sinc RF pulse has a bandwidth of approximately 1.5 kHz, which would require a 3.5 G/cm slice selection gradient. The gradient amplifiers that will be used can output a maximum of 10 A, so the required gradient efficiency would be .35 G/cm/A.

The MATLAB simulations showed that the gradient set as designed would have an efficiency of .00928 G/cm/A for a single winding. This would require a gradient with 38 windings, which seemed a little excessive for a compact, low cost gradient set. The requirements were then relaxed by a factor of approximately 2, with the reasoning being that at low fields, a 1 mm slice thickness would produce so little signal as to be nearly unusable. A gradient set with 20 turns on each coil was chosen, which can generate with a 10 A pulse a 1.85 mm slice thickness, which is still very thin.

Gradient Construction

The gradients were wound by hand on a pair of square acrylic sheets. The dimensions of each coil were marked on the sheets, then nylon screws were driven into the sheet to wind the coils on. Because the gradients are pulsed with fairly large currents, a substantial transverse force is exerted on the wire segments. The gradients were tested without any restraint on the windings, and the force generated was significant enough to cause the windings to vibrate substantially but not enough to damage the coil. Wound gradient coils are often potted in epoxy or resin, but it was decided that simply fixing the windings to the acrylic former with cable ties would be sufficient. The single-axis gradient set can be seen in figure III.6.

After the first coil was wound, its resistance and inductance were measured and found to be 3Ω and $550\mu H$. The two sides of the gradient were wired in series, giving a combined

Fig. III.6. Single-axis gradient set as constructed

impedance of 6Ω and $1100\mu H$. The coils can be driven in parallel, halving the resistance and inductance (1.5Ω and $225\mu H$), but this comes at the cost of the current efficiency (G/cm/A) being reduced by a factor of two.

After the first gradient was constructed, it was tested to verify the strength of the gradient field. This was done as before, using the projection of a small vial of water at two positions within the coil to measure the strength of the gradient field. The coil was displaced by only 1 cm between measurements, as it was important that the coil remain within the homogeneous region of the gradient field. This physical shift generated a 1.9 kHz frequency shift, which corresponds to a gradient strength of .19 G/cm/A, which is within rounding error of the predicted gradient strength.

RF Gradiometer Coil

The new gradient set was too small to allow the use of the RF shield that had been previously used. Imaging was attempted using an RF coil without any sort of shielding, but the noise levels were simply too high to allow any usable images to be acquired. Some form of RF shielding was necessary to reduce the noise levels to a level that would allow imaging. This could be done by constructing an RF shield, but this was decided to be contrary to the aim of this project. RF shields are bulky and prevent easy access to the RF coil. In clinical MRI systems, the entire imaging room is RF shielded, but this simply is not possible for a low cost imaging system. Instead, a different approach was chosen – the construction of a RF Gradiometer Coil.

Gradiometers are commonly used in ultra low field (μT) MRI along with SQUID (superconducting quantum interference device) coils to perform imaging. [20] [21]. At higher fields, the extremely sensitivity of SQUID detectors is unnecessary, but the noise advantages of the gradiometer coil arrangement are still valuable. The gradiometer coil constructed consists of two multi-turn loops wound in series on the same cylindrical former, some distance apart.

The second loop is wound in the opposite direction as the first, so that any signals common to both loops cancel. The sample is placed within the first loop, and the loops are spaced sufficiently far apart that the sample should generate a substantial signal in the first coil, but very little in the second. Noise, however, should be relatively constant across the volume of the coil, and thus should cancel itself out because it generates opposite responses in each of the opposed loops.

In order to determine the proper spacing of the two coils of the gradiometer, a simulation was performed in MATLAB. Because of the coils are small electrically, a static approximation can be made for the fields generated by the coils. Solving for the on-axis fields of a circular loop is trivial, but it was desired to know the fields generated by the loops at any arbitrary point within the coil. In order to do this, the Biot-Savart Law must be integrated around the loop with a angle-dependent radius.

$$\mathbf{B} = \frac{\mu_0 I R}{4\pi} \int_0^{2\pi} \frac{\hat{x} z \cos\theta + \hat{y} z \sin\theta + \hat{z}(R - x\cos\theta - y\sin\theta)}{(R^2 + x^2 + y^2 - 2xR\cos\theta - 2yR\sin\theta + z^2)^{3/2}} d\theta \qquad \text{(III.3)}$$

Where R is the coil radius. This can be simplified into a form involving elliptic integrals, but this is far less intuitive. Unlike the Biot-Savart Law solution for straight wire segments, simulation of the round coils using this integral is quite computationally intensive, and the computation of the result for a 100x100 matrix of points requires a substantial amount of time. Fortunately, because the coil configuration is rotationally symmetric, it is possible to thoroughly characterize the behavior of the coil by simulating over a 2-D grid in only the Y and Z directions.

Coil Construction and Characterization

In order to demonstrate the RF Gradiometer coil's performance, two coils were constructed. The first coil is a simple loop with 10 turns of enameled wire laying side by side on an a cylindrical former. The gradiometer was constructed on the other end of the same former. It

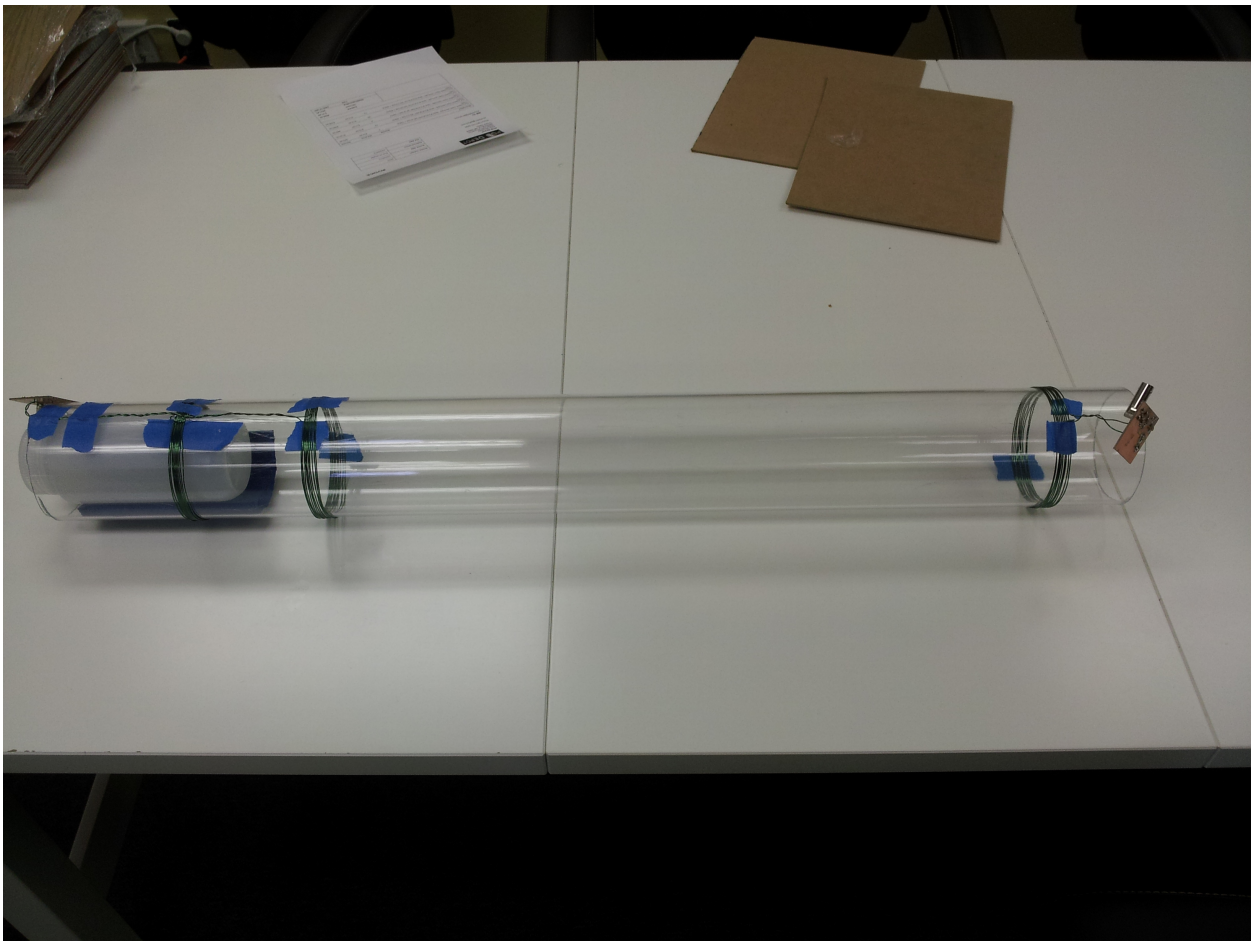

Fig. III.7. Former with both gradiometer and single loop coils. The water bottle phantom used for test imaging is inside the gradiometer coil.

consists of two loops identical to the first coil connected in series and separated by a distance of . The former with both coils on it can be seen in figure III.7. Detail of the gradiometer coil can be seen in figure III.8.

Both of the coils were then matched and tuned to 50Ω using fixed and variable capacitors in a T network. To demonstrate the noise-rejection performance of the gradiometer, two experiments were performed. First, the gradiometer coil was placed inside of a larger, longer solenoidal coil, and the S_{21} of the two coils was measured. By adjusting the position of gradiometer within the larger solenoid, it was possible to find a position where the gradiometer

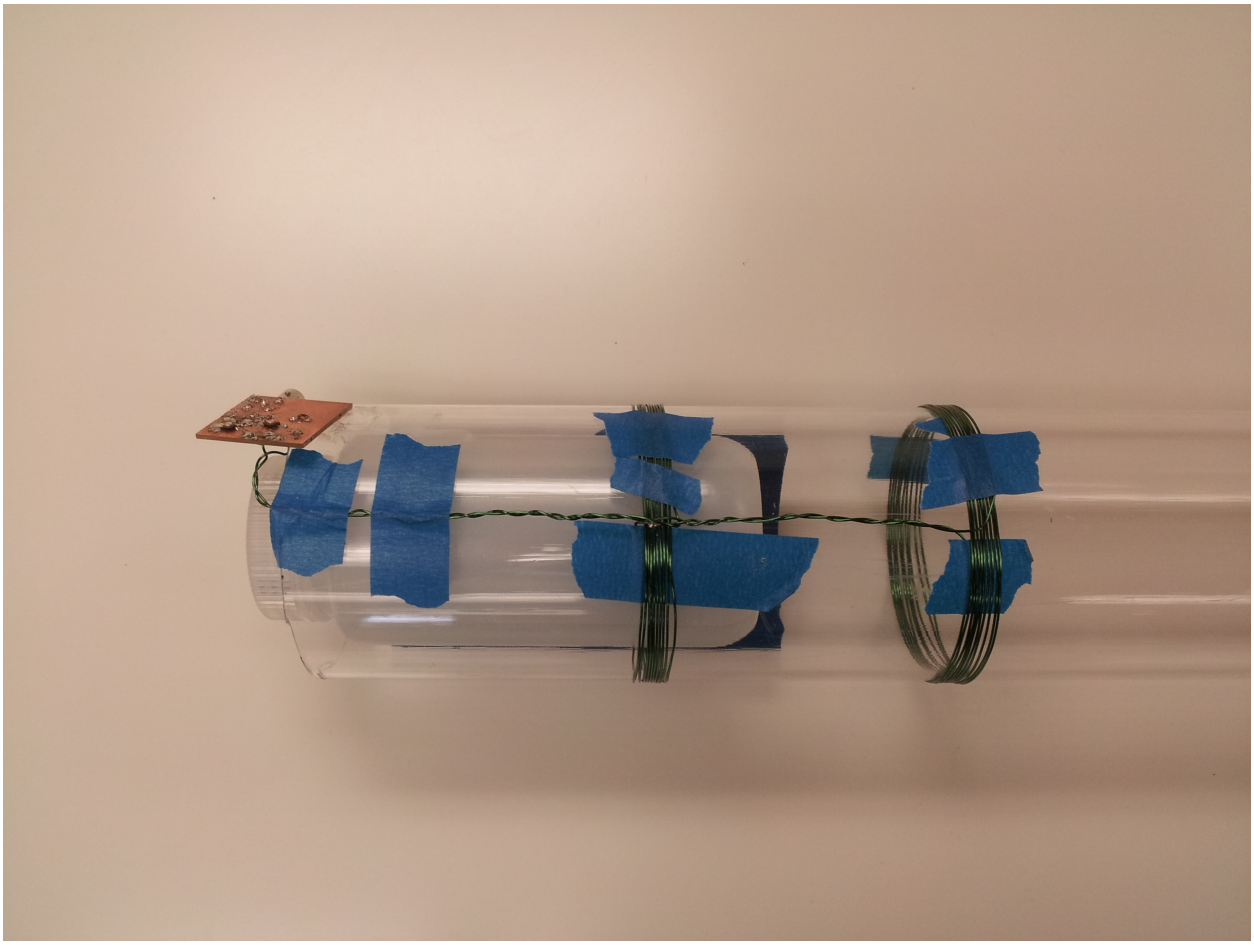

Fig. III.8. Detail of the gradiometer coil. The water bottle phantom is placed inside only one of the loops to generate the noise cancelling effect.

was centered within the larger coil where S_{21} dropped to practically zero. Because the large solenoid generates a nearly homogeneous field, this demonstrates that the oppositely wound loops generate canceling signals when exposed to a uniform field.

The second experiment was a quantitative comparison of the behavior of the gradiometer and standard loop coils when excited with a source a significant distance away. A network analyzer was configured to make an S_{21} measurement. The RF coil was connected to port 2 by means of an LNA, which was used to boost the signal to a usable level. Port 1 was connected to a small loop probe which was mounted on an acrylic rod, allowing its distance from the coil to be easily adjusted and quickly reproduced (figure III.9). The analyzer was not calibrated due to the nature of the setup, so the measurements are only valid in a relative sense.

The probe was placed 27 cm from the coil. The S_{21} for the simple coil was measured to be -15 dB at 2.46 GHz. When the gradiometer coil was measured in a similar fashion, S_{21} was measured to be -21 dB. Although these numbers are a good indication of the functioning of the gradiometer coil, the measurement is still flawed in many ways, as the coil probe is not truly in the far field of the gradiometer coil, so the two loops are not identically illuminated. Regardless, it gives a good quantitative demonstration of the coil's performance.

Coil Imaging Results

To verify performance of the gradiometer coil, it was used in the .06T permanent magnet with conjunction with the constructed single-axis gradient to acquire projections and images. Because acquisition of projections is more robust and requires less time, the functionality of the coil was first verified with projections in the Y direction. The phantom used was a Nalgene bottle mostly filled with distilled water that mostly filled the coil. The bottle was placed within the first coil of the gradiometer, leaving the second open to cancel out any external noise.

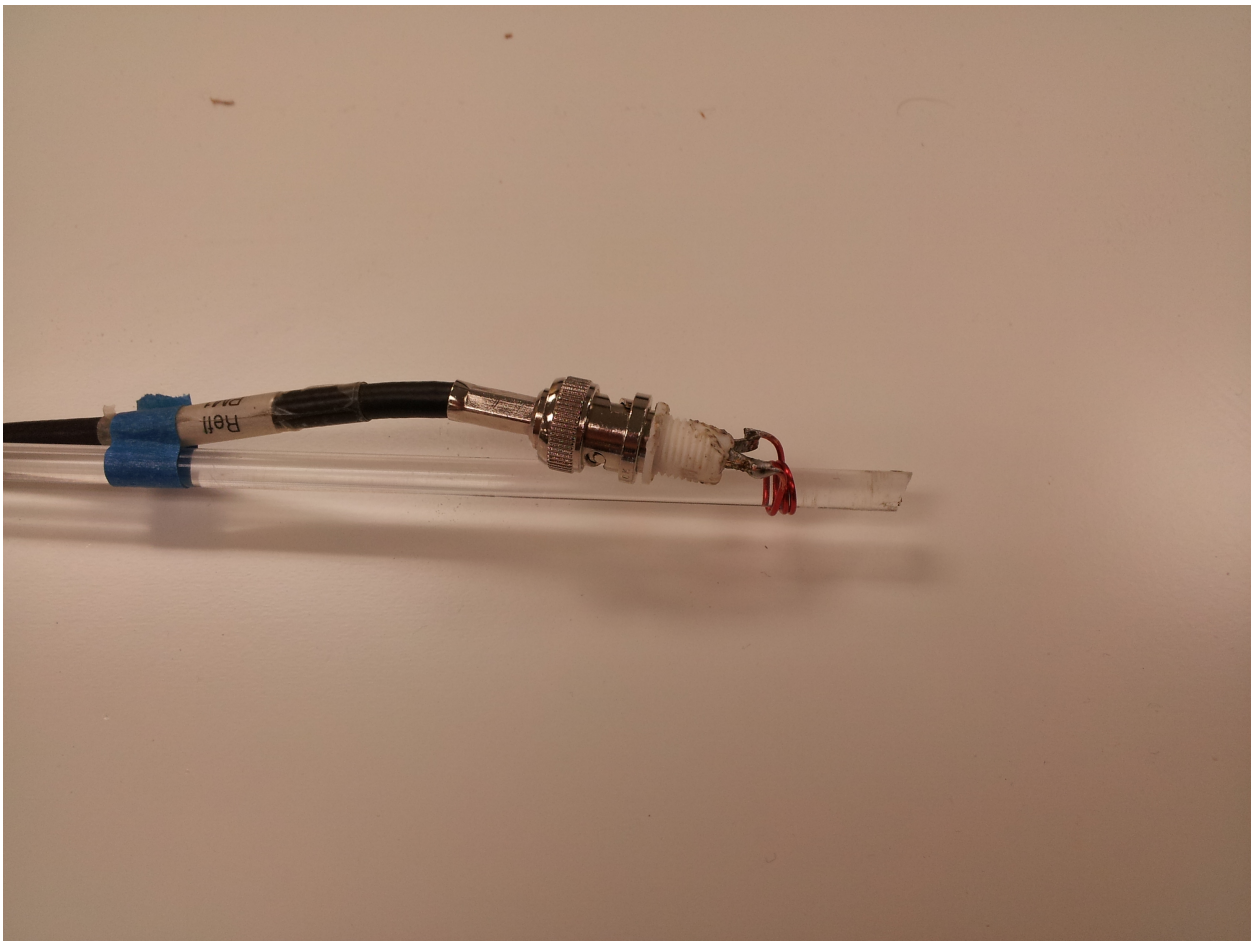

Fig. III.9. Small coil probe used to test noise rejection by gradiometer coil.

Projections

All of the projections and images were taken with TE = 20ms and TR = 4s. The first projection (figure III.10) was taken with 128 points over a 500mm field of view. No slice selection was performed. 64 averages were taken to ensure a high SNR. Although it is less obvious in the averaged image, there is are noise sources just to the right of the bottle that were coherent enough not to average out completely. A second projection (figure III.11) was taken at higher resolution, with 128 points over a 250mm field of view, also with no slice selection. As is expected, the phantom is wider in the projection, but less intense.

An additional projection was taken using the same field of view as the first (128 points over 500mm) with a 1cm slice selected, which can be seen in figure III.12. Other than slice selection, the parameters are identical to those used to acquire figure III.10. When the two projections are compared, it is clear that slice selection greatly reduces SNR, as the peak of the slice selected projection is less than one-tenth that of the plain projection.

Imaging

Because this is MRI, it was necessary to test the gradiometer's performance with imaging. The first image was acquired with an imaging matrix 64 square over a 500mm square field of view. The same TE and TR were used as in the projections, and four averages were taken. No slice select was used. The reconstructed image can be seen in figure III.13. The image is low-resolution with a large FOV, but the clipped circle of the partially full water bottle can still be clearly seen in the center of the image. The bands of noise that were visible in the projections are still visible in this image. They are more severe in the image than the projections because of the lower number of averages used in the image. Images could be acquired with more averages to reduce the visibility of the noise, but it quickly becomes too time consuming to be practical.

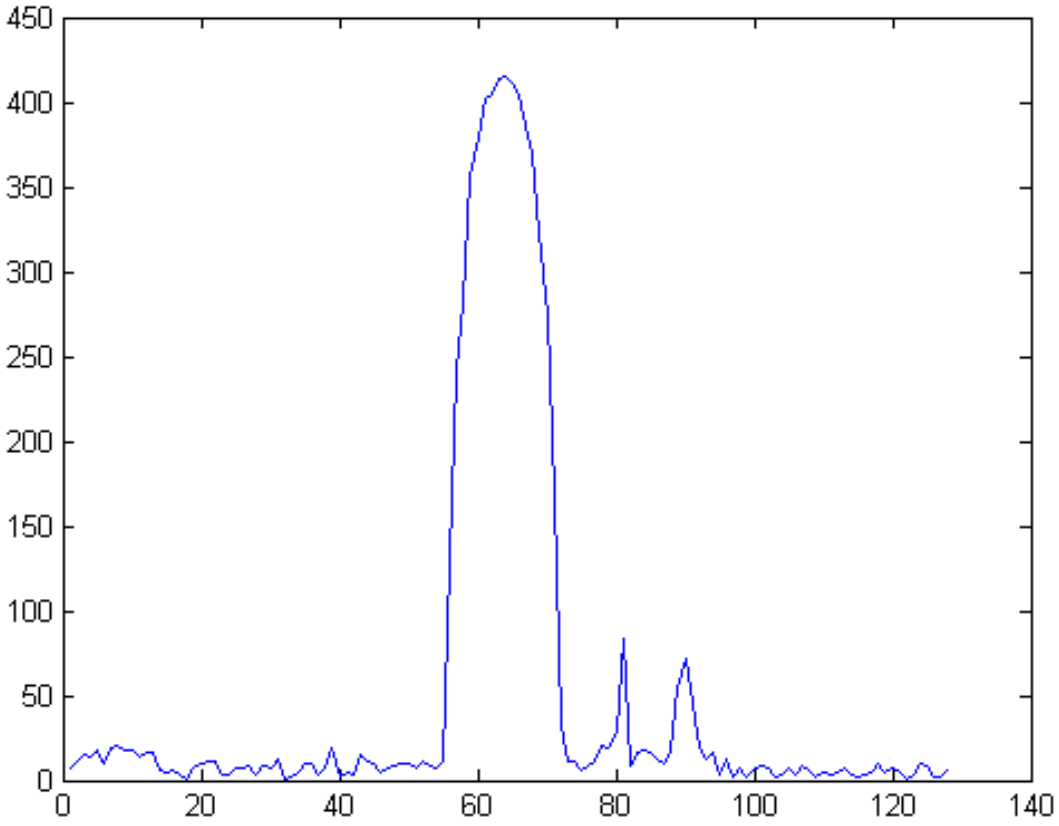

Fig. III.10. Projection taken in gradiometer coil with 128 points over a 500mm field of view.

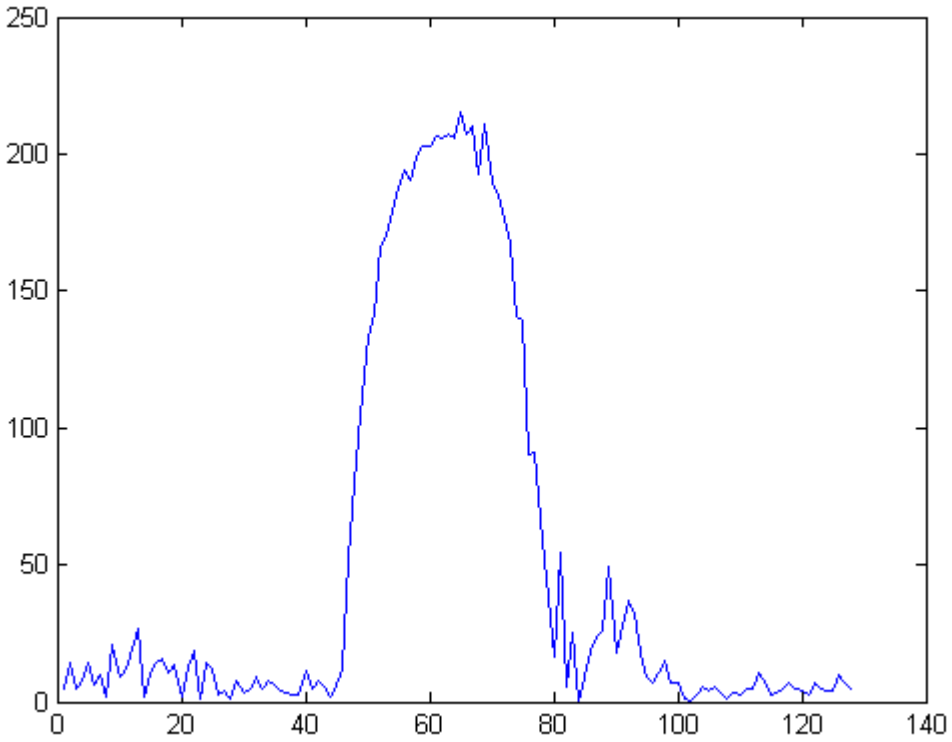

Fig. III.11. Projection taken in gradiometer coil with 128 points over a 250mm field of view.

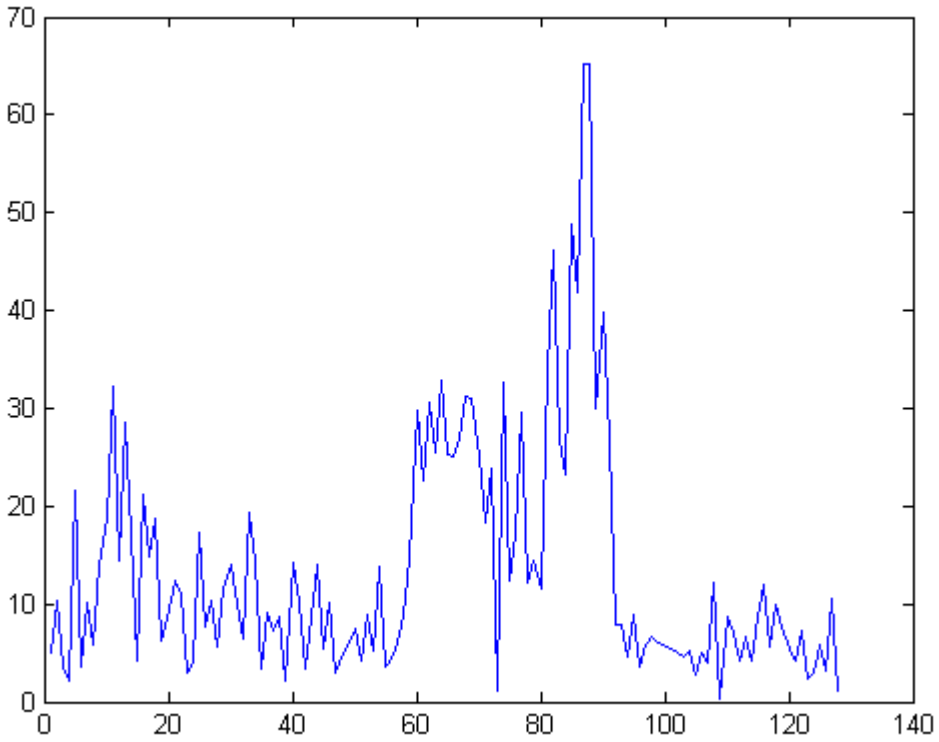

Fig. III.12. Projection taken in gradiometer coil with 128 points over a 500mm field of view and a 1cm slice thickness.

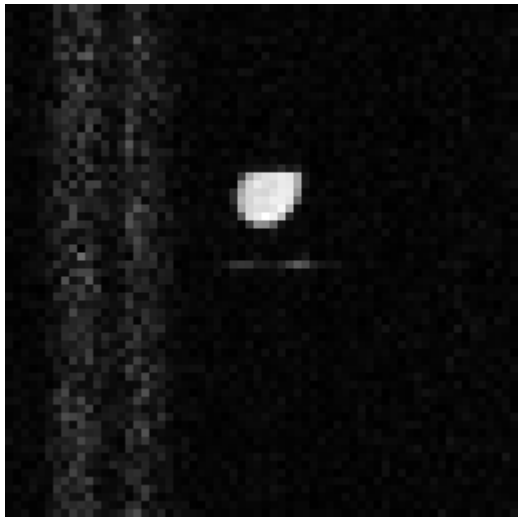

Fig. III.13. Image acquired in gradiometer coil with no slice selection.

CHAPTER IV
FRINGE FIELD EXPERIMENTS

The final experiments performed with the desktop MRI system were conducted in the fringe field of a 40cm 4.7 superconducting magnet. The aim of these experiments was to demonstrate the functioning of the desktop spectrometer with a coil in the fringe field of a superconducting magnet. Working in the fringe field creates several difficulties, as the magnetic field has a strong permanent gradient (approximately 10 G/cm) , which makes echoes short and difficult to find.

System Setup

A Hall Effect probe was used to find the approximate location where the fringe field is .06 T – the same as the permanent magnet. A very small RF coil and phantom (approximately 1cm wide) were placed in that location, and then an effort was made to find the center frequency at that point. When finding the center frequency, it is helpful to use as short an RF pulse as possible, as a shorter pulse will excite spins over a broader bandwidth, making the center frequency easier to find. The same setup was tested in the .06T permanent magnet to verify its correct functioning. A 10μs pulse at the amplifier's maximum power (about 20 W) was successful in exciting a bandwidth of at least 100 kHz.

The coil and phantom were then relocated to the fringe field of the magnet. The field at the phantom's location was checked again before beginning to hunt for an echo. A great deal of time was spent exciting the phantom at different frequencies and adjusting the position of the phantom in the fringe field. The Hall probe used wasn't terribly accurate, so it was thought that making small adjustments to the phantom's position would enable an echo to be found.

Problem Analysis

After a great deal of time was spent searching for an echo using the above method, it was decided to give the problem further thought. The primary concern was the gradient, so time was taken to map it over a range surrounding the .06T point in the fringe field (figure IV.1). Examining this data, it is clear that the gradient at the .06T point is about 10 G/cm. This strong gradient can cause several problems, the most significant being the widening of the spectral line produced by the phantom. The strong constant gradient causes constant motion in k-space. The result of this is that even without any external gradients, any spin echo is actually a projection in the direction of the permanent gradient.

Knowing the approximate gradient strength and phantom size, the expected linewidth can be calculated. With a 10 G/cm gradient and a 1 cm phantom, the following dimensional analysis yields an expected linewidth of:

$$\Delta f = 1\text{cm} \cdot \frac{10\text{G}}{\text{cm}} \cdot \frac{42.58\text{MHz}}{10000\text{G}} = 42.58\text{kHz} \tag{IV.1}$$

With the SNR available at .06T on our system, this large of a linewidth simply results in any echo being undetectable. The energy in the signal that was detected in the permanent magnet is now spread over a much wider bandwidth. The smaller signal that is then produced is below the noise floor of the system, making detection impossible. With sufficient averaging, it is theoretically possible to extract an echo buried in noise, but due to the difficulties already present in finding the center frequency in a rapidly varying field, this approach was not pursued.

Thoughts for Future Work

Although this particular experiment was not successful in producing a detectable echo, it was highly instructive. Because a large phantom produces a large linewidth, in future ex-

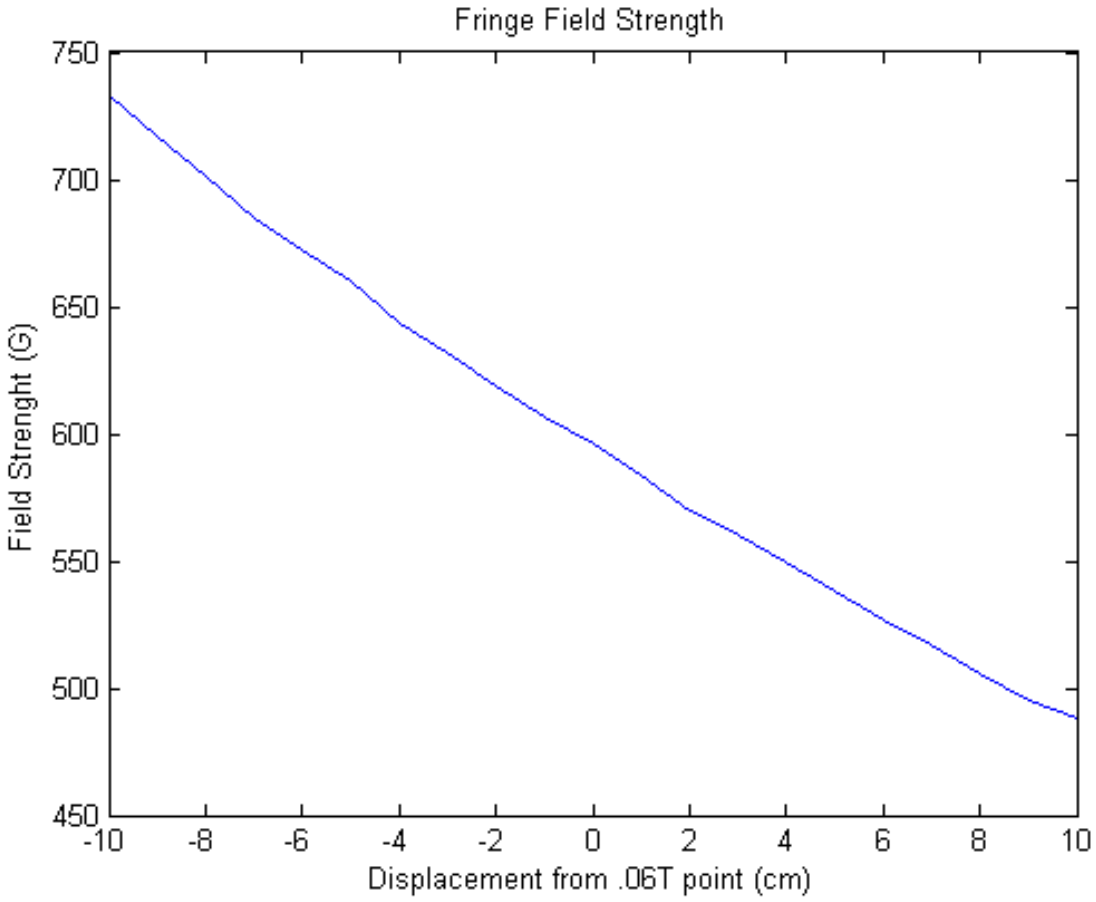

Fig. IV.1. Fringe field strength around .06T field point.

periments, it would be wise to use as small a phantom as possible. In addition, the small phantom should be in a highly efficient coil in order to extract the most signal possible out of the phantom. One attractive idea for a coil-phantom combination is a solenoidal coil of wire wrapped around a capillary tube filled with water.

Another lesson learned was the importance of verifying correct system performance in a known magnet before searching for an echo in the fringe field. By checking the system and performing RF pulse strength calibration in a known magnet, many unknowns can be eliminated from the fringe field test setup.

REFERENCES

[1] M. Stehling, R. Turner, P. Mansfield, *et al.*, "Echo-planar imaging: magnetic resonance imaging in a fraction of a second," *Science*, vol. 254, no. 5028, pp. 43–50, 1991.

[2] P. Lauterbur *et al.*, "Image formation by induced local interactions: examples employing nuclear magnetic resonance," *Nature*, vol. 242, no. 5394, pp. 190–191, 1973.

[3] J. Hajnal, D. Bryant, L. Kasuboski, P. Pattany, B. De Coene, P. Lewis, J. Pennock, A. Oatridge, I. Young, G. Bydder, *et al.*, "Use of fluid attenuated inversion recovery (FLAIR) pulse sequences in MRI of the brain.," *Journal of computer assisted tomography*, vol. 16, no. 6, p. 841, 1992.

[4] G. Glover and E. Schneider, "Three-point dixon technique for true water/fat decomposition with B0 inhomogeneity correction," *Magnetic resonance in medicine*, vol. 18, no. 2, pp. 371–383, 2005.

[5] G. E. Wesbey, M. E. Moseley, R. L. Ehman, *et al.*, "Translational molecular self-diffusion in magnetic resonance imaging. ii. measurement of the self-diffusion coefficient.," *Investigative radiology*, vol. 19, no. 6, p. 491, 1984.

[6] J. Carlson and T. Minemura, "Imaging time reduction through multiple receiver coil data acquisition and image reconstruction," *Magnetic resonance in medicine*, vol. 29, no. 5, pp. 681–687, 2005.

[7] D. Sodickson and W. Manning, "Simultaneous acquisition of spatial harmonics (SMASH): fast imaging with radiofrequency coil arrays," *Magnetic Resonance in Medicine*, vol. 38, no. 4, pp. 591–603, 2005.

[8] K. Pruessmann, M. Weiger, M. Scheidegger, P. Boesiger, *et al.*, "SENSE: sensitivity encoding for fast MRI," *Magnetic Resonance in Medicine*, vol. 42, no. 5, pp. 952–962, 1999.

[9] M. McDougall and S. Wright, "64-channel array coil for single echo acquisition magnetic resonance imaging," *Magnetic resonance in medicine*, vol. 54, no. 2, pp. 386–392, 2005.

[10] A. Macovski and S. Conolly, "Novel approaches to low-cost mri," *Magnetic resonance in medicine*, vol. 30, no. 2, pp. 221–230, 1993.

[11] J. Jackson, L. Burnett, and J. Harmon, "Remote (inside-out) NMR. iii. detection of nuclear magnetic resonance in a remotely produced region of homogeneous magnetic field," *Journal of Magnetic Resonance (1969)*, vol. 41, no. 3, pp. 411–421, 1980.

[12] B. Blümich, P. Blümler, G. Eidmann, A. Guthausen, R. Haken, U. Schmitz, K. Saito, and G. Zimmer, "The NMR-mouse: construction, excitation, and applications," *Magnetic resonance imaging*, vol. 16, no. 5, pp. 479–484, 1998.

[13] F. Casanova and B. Blümich, "Two-dimensional imaging with a single-sided NMR probe," *Journal of Magnetic Resonance*, vol. 163, no. 1, pp. 38–45, 2003.

[14] J. Godward, E. Ciampi, M. Cifelli, and P. McDonald, "Multidimensional imaging using combined stray field and pulsed gradients," *Journal of magnetic resonance*, vol. 155, no. 1, pp. 92–99, 2002.

[15] J. Prince and J. Links, *Medical Imaging Signals And Systems*. Pearson Prentice Hall Bioengineering, Pearson Prentice Hall, 2006.

[16] S. Wright, D. Brown, J. Porter, D. Spence, E. Esparza, D. Cole, and F. Huson, "A desktop magnetic resonance imaging system," *Magnetic Resonance Materials in Physics, Biology and Medicine*, vol. 13, no. 3, pp. 177–185, 2001.

[17] C. Hayes, W. Edelstein, J. Schenck, O. Mueller, and M. Eash, "An efficient, highly homogeneous radiofrequency coil for whole-body nmr imaging at 1.5 t," *Journal of Magnetic Resonance*, vol. 63, no. 3, pp. 622–628, 1985.

[18] W. Anderson, "Electrical current shims for correcting magnetic fields," *Review of Scientific Instruments*, vol. 32, no. 3, pp. 241–250, 1961.

[19] R. Turner, "A target field approach to optimal coil design," *Journal of physics D: Applied physics*, vol. 19, no. 8, p. L147, 2000.

[20] W. Myers, D. Slichter, M. Hatridge, S. Busch, M. Mößle, R. McDermott, A. Trabesinger, and J. Clarke, "Calculated signal-to-noise ratio of mri detected with squids and faraday detectors in fields from 10μt to 1.5 t," *Journal of Magnetic Resonance*, vol. 186, no. 2, pp. 182–192, 2007.

[21] B. Suits, A. Garroway, and J. Miller, "Surface and gradiometer coils near a conducting body: the lift-off effect," *Journal of magnetic Resonance*, vol. 135, no. 2, pp. 373–379, 1998.